Growth and characterization of Tb silicide nanostructures on Si(*hhk*) substrates

Stephan Appelfeller,[1,*] Martin Franz,[1] Lars Freter,[1,2] Christian Hassenstein,[1] Hans-Ferdinand Jirschik,[1] and Mario Dähne[1]

[1]*Institut für Festkörperphysik, Technische Universität Berlin, 10623 Berlin, Germany*

[2]*Peter Grünberg Institut, Forschungszentrum Jülich GmbH, 52425 Jülich, Germany*

(Received 23 September 2019; published 11 December 2019)

The growth of Tb-induced nanostructures on vicinal Si(111) substrates with an offcut toward the [11$\bar{2}$] direction, so-called Si(*hhk*) substrates, was studied. The nanostructures were analyzed using scanning tunneling microscopy and spectroscopy as well as core-level photoemission spectroscopy. For low Tb coverages, terraces covered by a Tb-induced submonolayer structure are observed. At higher coverages, metallic Tb disilicide monolayer structures are dominant. Their appearance strongly depends on the offcut direction. Well-defined nanowires with straight edges are only present for Si(*hhk*) substrates with $h < k$. Furthermore, only these substrates may host very narrow metallic nanolines. In general, narrower nanostructures are observed for larger offcut angles enabling the formation of Tb disilicide nanowires with average widths as low as 2.3 nm for Si(335) substrates.

DOI: 10.1103/PhysRevMaterials.3.126002

I. INTRODUCTION

Low-dimensional materials are fascinating systems showing physical properties vastly different from three-dimensional bulk materials. Electron correlations are stronger with reduced dimensionality, leading to the breakdown of the Fermi liquid theory in one dimension [1]. Characteristic properties of such one-dimensional materials include Tomonaga-Luttinger liquid behavior [2–6], spin-charge separation [7,8], and the Peierls transition [9–11]. All materials showing one-dimensional characteristics have in common that they are not purely one-dimensional systems, but are stabilized by their three- or two-dimensional environment, e.g., by coupling of multiple parallel chains or by using a substrate. Thus, these materials are denoted quasi-one-dimensional [1,12].

There are several ways to grow quasi-one-dimensional materials on a surface. They may form by self-organization due to anisotropic properties of the planar substrate or the grown nanostructures [13–23] or their growth may be promoted by vicinal substrates leading to linear surface structures at steps or on terraces [24–33]. The latter approach is illustrated in Fig. 1 for the case of a rare-earth disilicide layer forming on (111) terraces of a stepped Si(111) substrate.

Such monolayers of hexagonal rare-earth disilicides on planar Si(111) substrates are two-dimensional metals with heights of only about 0.4 nm, well-known electronic structures, and very intriguing physical properties [34–40]. Initially, the research focused on their electronic properties. The observation of extremely low Schottky barrier heights on *n*-type Si make them interesting, e.g., for ohmic contacts [34–36]. Recently, their magnetic properties came into focus since they are the first-known materials showing intrinsic two-dimensional in-plane ferromagnetism possibly leading to new spintronic devices [39,40].

The possibility to confine the two-dimensional silicides by using a substrate vicinal to Si(111) has already been demonstrated [30–32]. However, only the combinations of Si(557) substrates with Dy or Er as rare earth were used and rather broad nanowires with widths of about 10 nm were observed. Here, we report on the formation of linear Tb silicide surface structures on various substrates being vicinal to Si(111) and their characterization by scanning tunneling microscopy (STM) and spectroscopy (STS) as well as by core-level photoemission spectroscopy (XPS). In this study, mainly the Tb coverage was varied from submonolayer coverages up to a coverage typical for the preparation of a Tb disilicide monolayer on planar Si(111) substrates. The annealing procedure necessary for the formation of the nanostructures was similar as the one for the Tb disilicide monolayer on planar Si(111) substrates.

The hexagonal rare-earth disilicides form edges preferentially along the $\langle\bar{1}10\rangle$ directions, corresponding to a minimum dangling bond density. To promote the formation of Tb disilicide structures with straight edges, vicinal substrates with different offcuts toward the perpendicular [11$\bar{2}$] direction are chosen in this paper [see Fig. 1(b)], which are denoted as Si(*hhk*) substrates.

Indeed, nanostructures with straight edges are found here for Si(*hhk*) substrates with $h < k$. In the studied Tb coverage regime, three different types of dominating surface structures are observed. There are metallic nanowires consisting of the Tb disilicide monolayer with average widths down to 2.3 nm at appropriate preparation conditions, terraces covered by a Tb-induced submonolayer structure, and nanolines that are less than 1 nm wide.

When using Si(*hhk*) substrates with $h > k$, the Tb-induced submonolayer and monolayer structures are also found, but nanolines are not observed. Furthermore, both the

*Corresponding author: stephan.appelfeller@physik.tu-berlin.de

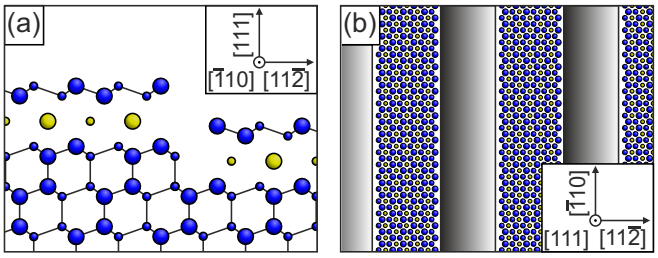

FIG. 1. (a) Structure model shown in side view of a rare-earth disilicide monolayer on Si(111) disrupted by a monoatomic step running in the [$\bar{1}$10] direction. (b) Schematic top view of rare-earth disilicide nanowires on Si(*hhk*) substrates with steps indicated by color gradients from black to white. In (a) and (b), rare-earth and Si atoms are indicated by yellow and blue circles, respectively.

submonolayer and the monolayer structures now show rather rough edges, indicating a strong influence of the offcut direction on the nanostructure growth. Anyway, there is the expected trend to narrower nanostructures for larger offcut angles for both offcut directions.

II. EXPERIMENTAL DETAILS

The samples were cut from commercial *p*-type and *n*-type Si(*hhk*) wafers and cleaned in UHV by degassing for at least 12 h at 600 °C followed by repeated flash annealing up to 1150 °C. Afterward, the samples were slowly cooled down from about 850 °C with a rate of about 1 °C/s to achieve well-ordered clean substrates. An infrared pyrometer was used to measure the temperature of the resistively heated samples (accuracy ±20 °C and an emissivity setting of 0.67 for the complete temperature range).

For the formation of the silicide structures, Tb was evaporated from home-built electron-beam evaporators onto the samples held at room temperature followed by annealing at elevated temperatures for 2 min. The deposited Tb amount was determined by the deposition time and the deposition rate, which was measured using a quartz crystal microbalance (accuracy ±20%). In this paper, the Tb coverage is given in monolayers (ML), with 1 ML always corresponding to the surface atom density of planar Si(111) substrates (7.8×10^{14} atoms/cm^2) for better comparison between the different vicinal Si(111) substrates. During the entire preparation procedure, the pressure did not exceed 5×10^{-7} Pa, while the measurements were performed *in situ* in different chambers with base pressures below 1×10^{-8} Pa.

STM and STS experiments were carried out at the Technische Universität Berlin with a home-built STM setup operating at room temperature using a commercial SPECS Nanonis control electronics. Electrochemically etched W tips were used after cleaning in UHV by electron bombardment. For processing the STM images, the WSXM software was used [41]. STS spectra were taken as point spectra with the differential conductance measured simultaneously using a software lock-in amplifier.

XPS data were taken at the UE56/2 PGM-1 and UE56/2 PGM-2 beamlines at BESSY II (Helmholtz-Zentrum Berlin) using a different chamber system, which was equipped with a SPECS PHOIBOS 100-electron analyzer operating in normal emission geometry. Again, all data were obtained at room temperature.

III. RESULTS AND DISCUSSION

The fundamental requirement of any growth study is the use of well-defined substrates. Thus, the clean Si(*hhk*) substrates used for the Tb-induced nanostructure formation are discussed first. Afterward, STM results on the growth of the various nanostructures are presented separately for the two offcut directions before the nanostructures are further characterized and identified using STS and XPS. Finally, the influence of Tb segregation into the Si bulk is discussed.

A. The clean Si(*hhk*) substrates

Vicinal Si(111) surfaces with different offcut angles toward the [11$\bar{2}$] direction are used as substrates for the growth of Tb silicide nanostructures. Figure 2(a) shows a schematic view though a Si crystal, in which the substrates used in this study are highlighted. In total, four different substrates where deployed to investigate the influence of the offcut direction as well as the magnitude of the offcut angle. Si(775) and Si(553) represent substrates with positive offcut angles of +8.5° and +12.5°, respectively. In contrast, Si(557) and Si(335) have negative offcut angles of −9.5° and −14.4°, respectively. It should be noted that positive and negative offcut angles lead to nonequivalent step structures. This is apparent, e.g., by the number of dangling bonds at the step edge atoms of the unreconstructed substrates, which are highlighted by colors in Fig. 2(a) for the substrates used in this study. For Si(*hhk*) substrates with $h>k$, there is only one dangling bond per edge atom, in contrast to two dangling bonds for Si(*hhk*) substrates with $h<k$.

Significant differences between the two offcut directions are also observed by STM for the clean reconstructed surfaces. For the two negative offcut angles studied here, the surfaces show a regular arrangement of narrow (111) facets alternating with a step structure [see Figs. 2(b) and 2(c)]. In most cases, the (111) facets contain only a single row of 7×7 unit cells, as they are known from planar Si(111) substrates. However, the distance between neighboring (111) terraces is larger for increasing absolute value of the offcut angle, i.e., the larger inclinations of the (111) terraces with respect to the nominal surface have to be compensated by wider step structures. These findings are in good agreement with the literature [42–45].

In contrast to the rather similar appearance of the substrates with negative offcut angles, there is a larger variety for the positive offcut angles studied here. For the clean Si(775) surface, shown in Fig. 2(e), wide (111) terraces containing multiple rows of 7×7 unit cells alternate with large areas of a fairly regular step structure. In contrast, no complete 7×7 unit cell is usually observed on Si(553) surfaces since there are only very narrow (111) facets forming a regular array [see Fig. 2(d)]. Again the observations made here are in good agreement with the literature [46,47].

In the following, it will be discussed if these apparent differences of the two offcut directions also lead to the growth of different nanostructures.

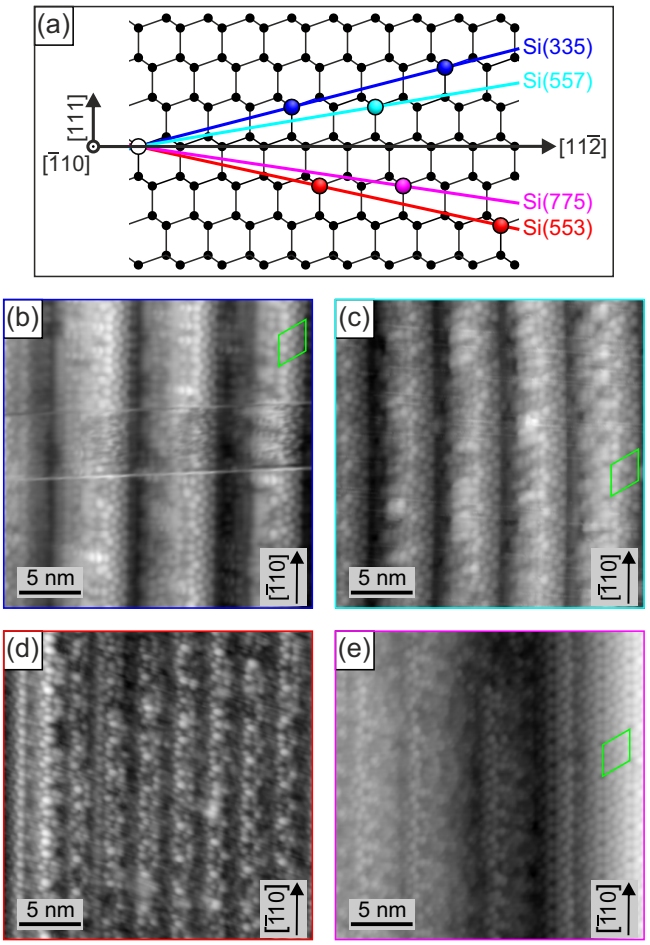

FIG. 2. (a) Schematic view through a Si crystal along the [$\bar{1}$10] direction with the vicinal Si substrates used in this study highlighted by colored lines. The black circles represent Si atoms, while the larger colored circles indicate Si atoms cut by the respective vicinal substrate planes. (b) to (e) STM images of the clean pristine surfaces of (b) Si(335), (c) Si(557), (d) Si(553), and (e) Si(775). The green rhombi in (b), (c), and (e) mark 7×7 unit cells. The sample biases (V) are (b) $+1.5$ V, (c) -1.5 V, (d) $+1.0$ V, and (e) -1.5 V, while the tunneling current (I) is 100 pA for all STM images shown in this paper.

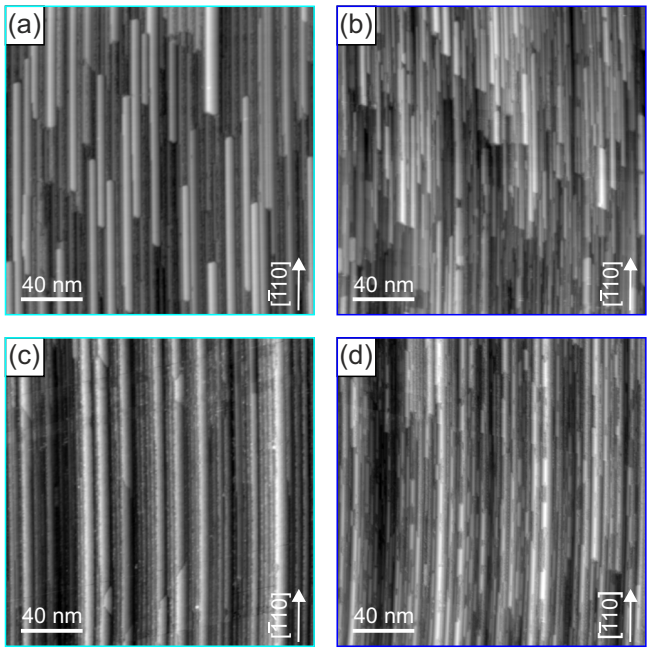

FIG. 3. (a) and (b) Overview STM images of preparations using (a) a Si(557) and (b) a Si(335) substrate and the typical preparation parameters for a closed Tb disilicide film on planar Si(111) substrates [Tb coverage $\Theta = 1.4$ ML and annealing temperature $T = 500\,^{\circ}$C for both preparations, (a) $V = -1.5$ V, and (b) $V = +1.5$ V]. (c) and (d) Overview STM images of preparations using only submonolayer amounts of Tb on (c) Si(557) and (d) Si(335) ($\Theta = 0.6$ ML, $T = 500\,^{\circ}$C, and $V = -1.5$ V for both samples).

B. Tb silicide nanostructure formation on Si(*hhk*)

The STM results on the Tb-induced nanostructures are presented separately for the two offcut directions starting with the substrates having negative offcut angles toward the [11$\bar{2}$] direction.

1. Si(hhk) substrates with h < k

The preparation parameters to obtain a closed Tb disilicide monolayer on planar Si(111) substrates are well known [17,37]. Due to Tb segregation into the Si bulk (see Sec. III D), slightly more than 1 ML has to be deposited and annealed at about 500 °C. Using this preparation procedure and a Si(557) substrate, highly elongated nanostructures extending in the [$\bar{1}$10] direction and characterized by straight edges are observed [see Fig. 3(a)]. Based on the appearance of the nanostructures as linear structures with lengths often exceeding 100 nm and with homogeneous widths, they are denoted as nanowires in this paper.

The nanowires on Si(557) have an average width of about 3.6 nm and their surfaces appear smooth, i.e., similar to Tb dislicide monolayers on Si(111) substrates for the used tunneling conditions [17,37]. Increasing the offcut with respect to Si(111), similar nanostructures are observed on Si(335) for the same preparation parameters [see Fig. 3(b)]. Due to the larger offcut, the nanowires are even narrower with average widths of 2.5 nm, but their growth is not as homogeneous as for the Si(557) substrate. On both substrates, the inclinations α of the nanowire surfaces with respect to the average substrate surfaces, $|\alpha_{\mathrm{Si}(557)}| = 9^{\circ} \pm 2^{\circ}$ and $|\alpha_{\mathrm{Si}(335)}| = 15^{\circ} \pm 2^{\circ}$, are in good agreement with the values expected for (111) facets, a further indication for Tb disilicide nanowires forming on (111) facets.

A deposition of less than 1 ML Tb on Si(*hhk*) substrates with $h < k$ leads to (111)-oriented terraces that are even narrower and longer than the nanowires observed for higher Tb coverages [see Figs. 3(c) and 3(d)]. However, these terraces are not uniformly covered with nanowires, but also show roughly appearing sections indicating the formation of a different surface structure. Thus, while the (111) terraces are on average much more extended in [$\bar{1}$10] direction, the nanowires are often rather short.

The difference between the nanowires and the roughly appearing structures is more apparent in the more detailed images shown in Fig. 4. Green arrows indicate nanowires

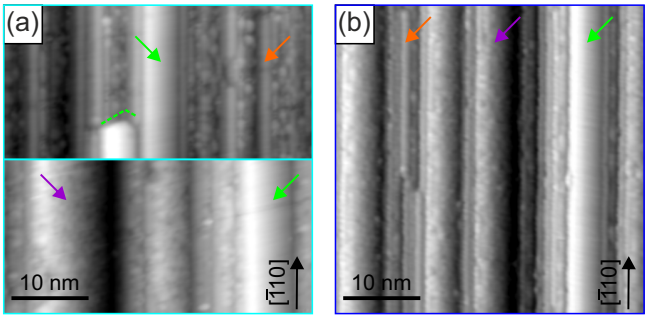

FIG. 4. Detailed STM images of the main structures observed on Si(557) and Si(335) being nanowires (marked by green arrows), rough terraces (marked purple), and nanolines (marked orange). (a) Si(557) substrate covered by 1.3 ML Tb (top) and 0.6 ML Tb (bottom) annealed at 500 °C (top $V = -1.5$ V and bottom $V = +1.5$ V). (b) Si(335) substrate covered by 0.6 ML Tb annealed at 500 °C ($V = -1.5$ V). The dashed line in (a) indicates $\langle \bar{1}10 \rangle$ directions.

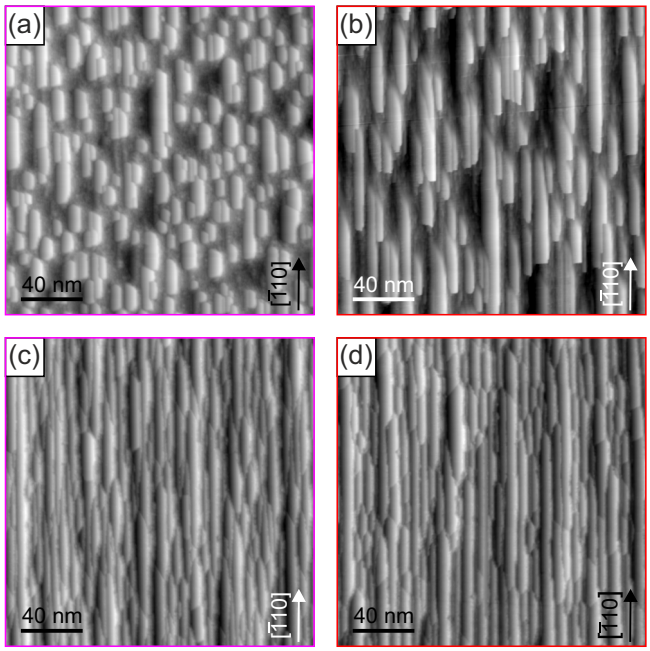

FIG. 5. Overview STM images of preparations on (a) and (c) Si(775) substrates and (b) and (d) Si(553) substrates using (a) and (b) Tb disilicide monolayer preparation parameters [$\Theta = 1.3$ ML, $T = 500$ °C, (a) $V = -2.5$ V, and (b) $V = -1.5$ V] and (c) and (d) submonolayer amounts of Tb (blank width) [$\Theta = 0.6$ ML, (c) $T = 500$ °C, (d) $T = 450$ °C, and $V = -1.5$ V for both images].

and purple ones roughly appearing (111) terraces. A Tb-induced surface structure known from planar Si(111) substrates with a similar rough appearance is the $2\sqrt{3}\times 2\sqrt{3}$ submonolayer [17,38]. The present observation that the density of the roughly appearing terrace sections increases with decreasing Tb coverage is in agreement with the assignment to a Tb-induced submonolayer structure. Unfortunately, there are no large domains with an apparent $2\sqrt{3}\times 2\sqrt{3}$ periodicity on the roughly appearing terrace sections, thus a conclusive assignment is not possible by STM alone. Similarly, atomic resolution was not achieved on the nanowires, preventing a definite assignment to the Tb disilicide. However, a further indication for the latter assignment are the edges at the nanowire ends predominantly lying in $\langle \bar{1}10 \rangle$ directions [see dashed green line in Fig. 4(a)].

In addition to the nanowires and the presumed Tb-induced submonolayer structure, there is another often occurring surface structure, which is marked by orange arrows in Fig. 4. Similar to the nanowires, these linear structures appear smooth but, with widths below 1 nm, they are much narrower than an average nanowire. In this paper, they are denoted nanolines. Due to their small widths and the convolution of the surface morphology with the STM tip structure in STM images, it is not possible to determine the surface orientation of the nanolines. Thus, they may form on a facet different from (111). Furthermore, it is not possible at the moment to determine if the nanolines are Tb-containing structures or if they consist purely of Si. Clean Si(337) facets, e.g., have a very similar appearance [42] and may be present here to achieve the average surface orientation in the presence of the rather wide (111) terraces.

2. Si(hhk) substrates with $h > k$

In the following, the STM results regarding the formation of Tb-induced nanostructures on Si(*hhk*) substrates with $h > k$ are presented.

Figures 5(a) and 5(b) show the nanostructure formation on Si(775) and Si(553), respectively, when using the preparation procedure to obtain a closed Tb disilicide monolayer on planar Si(111) substrates. Nanostructures with rather large widths often exceeding 10 nm and small lengths are observed. For the larger offcut angle, i.e., for the Si(553) substrate, the average aspect ratio of the nanostructures is slightly increased. However, the width of the nanostructures often drastically varies along the substrate steps. Thus, these nanostructures are not labeled nanowires, which would mean large aspect ratios and homogeneous widths. Instead, they are denoted as elongated islands in this paper.

For Si(*hhk*) substrates with $h < k$, an increase in (111) terrace length and a decrease in (111) terrace width were observed for submonolayer amounts of Tb. The same occurs for Si(*hhk*) substrates with $h > k$, where (111) terraces with lengths exceeding 100 nm are observed [see Figs. 5(c) and 5(d)]. Furthermore, similar to the observations for $h < k$, the (111) terraces are usually not covered homogeneously with a single type of surface structure. Taking a look at the detailed STM images shown in Fig. 6, there are again two different terrace sections with a smooth or rough appearance, which may be tentatively assigned to the Tb disilicide monolayer or the $2\sqrt{3}\times 2\sqrt{3}$ submonolayer, respectively. Due to the rather wide (111) facets, it was possible to obtain a better resolution on the roughly appearing terraces. Domain walls of the $2\sqrt{3}\times 2\sqrt{3}$ submonolayer structure appear to dominate these terraces [see the inset in Fig. 6(a)] [17,38,48].

The presumed Tb disilicide monolayer sections now have larger aspect ratios compared to the elongated islands. However, the width of these low coverage structures is still inhomogeneous. Thus, they are denoted as nanostripes to differentiate them from the nanowires observed at $h < k$ showing homogeneous widths. An analysis of the width of the nanostripes

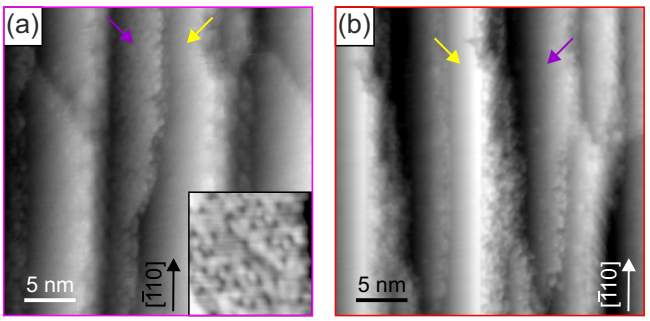

FIG. 6. Detailed STM images of the structures observed on Si(775) and Si(553) for low Tb coverages being nanostripes (marked by yellow arrows) and rough terraces (marked purple). (a) Si(775) substrate covered by 0.6 ML Tb annealed at 500 °C ($V = -1.5$ V) and (b) Si(553) substrate covered by 0.6 ML Tb and annealed at 500 °C ($V = -1.5$ V). The inset in (a) shows a 4-nm-wide area of a roughly appearing terrace.

at their widest extensions yields values of about 8 nm for nanostripes on Si(775) and of about 6 nm on Si(553), i.e., the nanostripes are narrower for larger offcut angles, in analogy to the observations made for nanowires on Si(*hhk*) substrates with $h < k$. Also similar to the nanowires, the inclinations of the nanostripe surfaces with respect to the average substrate surfaces, $|\alpha_{\mathrm{Si}(775)}| = 10^\circ \pm 2^\circ$ and $|\alpha_{\mathrm{Si}(553)}| = 12^\circ \pm 2^\circ$, are within their uncertainties in agreement with the values expected for (111) facets.

Another remarkable difference between both offcut directions is that no nanolines are observed for Si(*hhk*) substrates with $h > k$. This indicates that the formation of nanolines is not connected to (111) terraces, which are found for both offcut directions, but requires terraces or step structures having a negative offcut angle toward the [11$\bar{2}$] direction.

C. Identification of silicide structures

Up to now, the assignment of the observed structures is only based on their appearance in STM images. To confirm the proposed assignment, the structures were further analyzed using STS and XPS, as presented in the following.

1. Tunneling spectroscopy

An STS spectrum of the normalized differential conductance obtained by positioning the tip above a roughly appearing terrace on Si(335) is shown in Fig. 7(a) as a purple graph, together with an STS spectrum taken above a domain of the Tb-induced $2\sqrt{3}\times 2\sqrt{3}$ submonolayer on Si(111) shown in black. The course of both spectra is very similar, e.g., showing local maxima at about -1.3 V, slightly above 0 V, and at about $+0.8$ V. These results agree nicely with density-functional theory calculations [38]. Thus the STS results further prove the assignment of the roughly appearing terraces to the $2\sqrt{3}\times 2\sqrt{3}$ submonolayer. The main difference between both spectra is the decreased normalized differential conductance between -1.0 V and 0 V for the rough terraces. This discrepancy is related to the different tip stabilization conditions with the tip farther away from the sample for the submonolayer on the Si(335) substrate, leading to negligible current [see the $I(V)$ data in the inset in Fig. 7(a)].

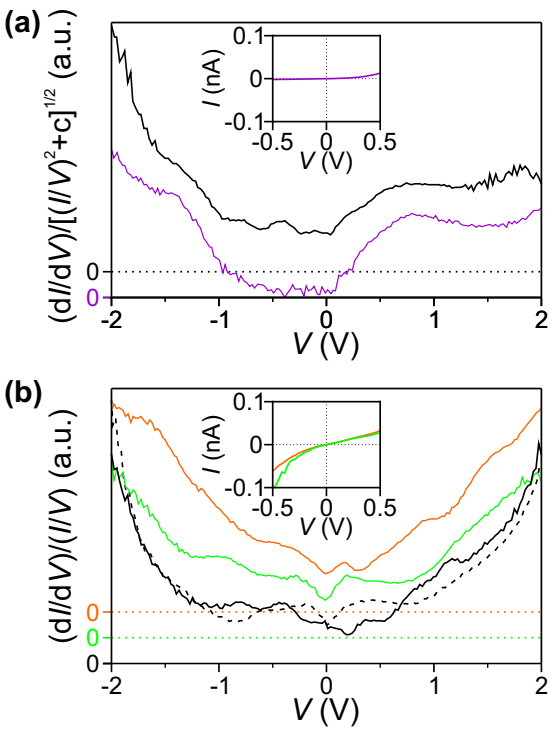

FIG. 7. (a) STS data taken on roughly appearing terraces on Si(335) in purple and on well-ordered domains of the Tb-induced $2\sqrt{3}\times 2\sqrt{3}$ submonolayer on Si(111) in black. Due to the wide voltage range with low current for the roughly appearing terrace [see inset], the normalized differential conductance was calculated in analogy to Ref. [49]. (b) STS data of the Tb disilicide monolayer on Si(111) as continuous black graph, the Tb silicide multilayer as dashed black graph, nanowires in green, and nanolines in orange. The insets show corresponding $I(V)$ curves.

For the nanowires and nanolines, in contrast, finite slopes are observed in the $I(V)$ curves around 0 V, as shown by the green and the orange graphs in the inset in Fig. 7(b), respectively. Such a metallic behavior is expected for nanostructures of the Tb dicilicide monolayer [37,38]. However, the normalized differential conductance of the nanowires and the Tb disilicide monolayer on Si(111) are distinctly different [compare green and black graphs in Fig. 7(b)]. Similarly, also the STS spectrum of the nanolines, shown in orange in Fig. 7(b), cannot be related well to the Tb disilicide monolayer on Si(111) substrates or to the nanowires. Furthermore, there is also no spectral agreement between nanowires or nanolines with the Tb silicide multilayer on planar substrates [dashed black graph in Fig. 7(b)]. Thus, a clear assignment of the nanowires or the nanolines to one of the silicide structures is not possible on the basis of the STS results alone. On the other hand, the STS data may be affected by a structured density of states of the tunneling tip or by electronic confinement due to the reduced width of the nanostructures, which may lead to the observed spectral deviations.

2. Core-level photoemission spectroscopy

While the electronic structure of a material might change by confinement, its chemical composition and consequently

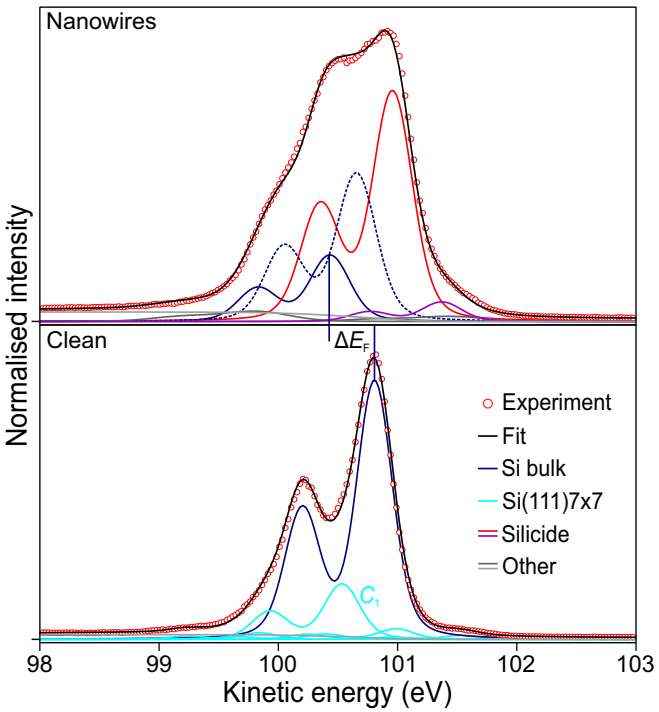

FIG. 8. Si-2p spectra of a clean Si(557) substrate and the same substrate after a nanowire preparation with deposition of 1.15 ML Tb and annealing at 500 °C ($h\nu = 200$ eV). The dashed Si bulk component in the nanowire spectrum corresponds to electrons from Si atoms not influenced by the nanowires.

the corresponding core-level spectra should be rather independent of such effects since they are dominated by local interactions. In the following, Si-2p spectra are analyzed. They are least squares fitted using spin-orbit split Voigt profiles to include both lifetime and instrumental broadening. A fixed spin-orbit splitting of 0.60 eV and a fixed intensity ratio of 2 : 1 are used to reduce the number of fit parameters. For every spectrum, a constant Lorentzian width of 0.10 eV (full width at half maximum) is used for all peaks. The Gaussian widths of the peaks were typically between 0.30 eV and 0.40 eV. A constant as well as a Shirley-type background are considered. The spectra of the same sample were fitted for different photon energies ($h\nu = 130$ eV, $h\nu = 160$ eV, and $h\nu = 200$ eV) until good results were obtained with differences of the chemical shifts of identical components below 0.01 eV. Si-2p spectra taken with $h\nu = 200$ eV have the least surface sensitivity, while measurements with $h\nu = 130$ eV are the most surface-sensitive ones, enabling an assignment of spectral components to bulk and surface Si atoms based on the dependence of their relative intensities on the photon energy.

Figure 8 shows Si-2p spectra for a clean Si(557) substrate and for one covered with nanowires. The spectrum of the clean surface can be fitted well by using the spectral composition known from planar Si(111) substrates [50]. In contrast to typical spectra of clean planar substrates, the relative intensity of the Si bulk component is strongly increased, in agreement with the reduced surface coverage by the 7×7 reconstruction. In addition, the so-called C_1 component is stronger for the vicinal substrate, which may be related to the step structure.

The Si-2p spectrum drastically changes upon nanowire preparation. In general, it can be fitted well using the known spectral composition for the Tb disilicide monolayer [37], but an additional weaker spectral component has to be included (marked purple), which lies about 0.40 eV higher in kinetic energy than the silicide component (marked red). This additional component may originate from a surface structure that is not significant on planar substrates.

Another difference between the nanowire spectrum and the typical Tb disilicide monolayer spectrum is the increased intensity of the Si bulk component attributed to substrate areas not influenced by nanowires (dashed dark blue component in Fig. 8). This is in good agreement with the observations made with STM. For the nanowire sample shown in Fig. 3(a), where typical preparation parameters for a complete coverage of a planar Si(111) substrate were used, only a fraction of the surface is covered by nanowires.

There is a second spectral component related to photoemission from the Si bulk (continuous dark blue in the upper part of Fig. 8). This Si bulk component is strongly shifted in energy with respect to the position of the Si bulk component found for the clean Si(557) substrate. Such a strong shift is expected for photoelectrons from below and the immediate surrounding of Tb disilicide monolayer structures due to the induced strong changes of the Fermi-level position in the Si band gap [37,38]. Interestingly, the corresponding shift of the Fermi level can be determined to $\Delta E_F \approx 0.37$ eV for the nanowire samples, which is even slightly larger than the value of $\Delta E_F \approx 0.33$ eV observed for planar substrates and corresponds to a Fermi-level position very close to the conduction band minimum of the Si substrate [37]. The resulting Fermi-level position upon Tb disilicide formation should be rather independent of the substrate orientation since the same (111) interface forms, but the initial Fermi-level position of the bare substrate may be different for vicinal substrates due to the influence of the steps.

The relative intensity of the shifted Si bulk component compared to the silicide component is rather low when compared with data for Tb disilicide films on planar substrates. This may be related to the fact that the Si(111) terraces with the nanowires are surrounded by steps leading to a reduced influence of the nanowires on the Fermi-level position in neighboring areas. In addition, there may be contributions at very similar kinetic energies as the silicide component, e.g., originating from Tb-induced structures at steps.

The good agreement between Si-2p spectra of the nanowire preparation on Si(557) and the Tb disilicide monolayer on Si(111) indicates the formation of Tb disilicide nanowires confirming the above assignment based on the STM data. Si-2p spectra of nanowire or nanostripe preparations using Si(335), Si(775), and Si(553) substrates are shown in Fig. 9. All spectra can be fitted well using the same spectral composition as found for the nanowire preparation on Si(557). Thus, also the narrower nanowires on Si(335) as well as the nanostripes on Si(hhk) substrates with $h > k$ consist of a Tb disilicide monolayer.

The additional component (colored purple) found for the nanowire preparation on Si(557), but not for the Tb disilicide monolayer on planar substrates is observed in all spectra. Consequently, it cannot be related to the presence of nanolines, which are only observed on Si(hhk) substrates with

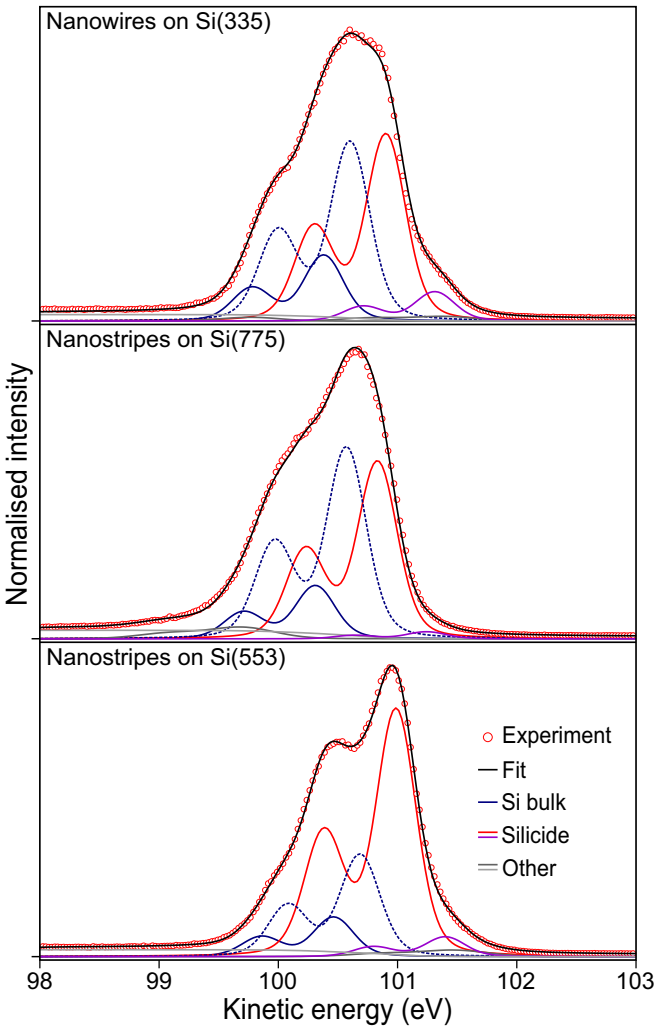

FIG. 9. Si-2p spectra of Tb silicide nanostructure preparations on Si(hhk) substrates using submonolayer Tb coverages ($h\nu = 200$ eV, $\Theta_{Si(335)} = 0.70$ ML, $\Theta_{Si(775)} = 0.55$ ML, $\Theta_{Si(335)} = 0.65$ ML, and $T = 500\,^{\circ}$C for all preparations). The dashed Si bulk components correspond to electrons from Si atoms not influenced by the nanowires.

$h < k$. Similarly, the terraces covered by the $2\sqrt{3}\times 2\sqrt{3}$ reconstructed submonolayer can be excluded since its surface coverage for the present nanowire preparation on Si(557) should be very low based on the STM data [see Fig. 3(a) and top part of Fig. 4(a)]. The only remaining common surface structure observed for both offcut directions is the Tb disilicide monolayer forming the nanowires and nanostripes. Thus, the purple colored component is presumably related to these structures.

In general, the relative intensity of this additional component increases with increasing offcut angle, i.e., for narrower nanostructures, and it is more pronounced for nanowires than for nanostripes. With decreasing width of the nanostructures, the relative contribution of the nanostructure edges increases. This behavior indicates that the additional component may be directly related to the straight edges in the [$\bar{1}$10] direction that are often disrupted for nanostripes. Such edges are also apparent for the Tb disilicide monolayer on planar substrates.

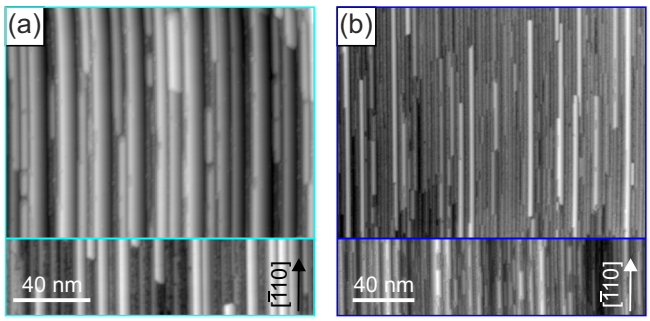

FIG. 10. (a) STM image of a reused Si(557) sample covered with 1.35 ML Tb for the second time ($T = 450\,^{\circ}$C and $V = +1.5$ V). (b) STM image of a reused Si(335) sample covered with 0.60 ML Tb for the third time ($T = 500\,^{\circ}$C and $V = -2.5$ V). The lower parts show STM images of the first identical preparations of nanowires on the same substrates.

However, the ratio of edge atoms to inner atoms is very low for these extended films, leading to a nondetectable edge-related Si-2p spectral component.

D. Tb segregation

The STM images showed surface coverages well below 1 ML, even when depositing slightly more than 1 ML Tb. Still, the grown structures consist of the Tb disilicide monolayer as proven by XPS. While further Tb-induced structures form on the surfaces, their heights do not indicate that they consist of multilayers leading to an actual Tb coverage below 1 ML. Thus, there is a finite Tb amount that is unaccounted for, which is discussed in the following.

The segregation of rare-earth atoms into the Si bulk during annealing procedures and their reaccumulation at the surface during cooling is well-known for Tb, Gd, and Y [37,51–54]. This means that no completely clean surface can be recovered by flash annealing after a preparation of Tb silicide nanostructures. This is, e.g., reflected by the observation that Si(hhk) substrates with $h < k$ show wider (111) terraces than at pristine samples. The additional Tb also leads to differences in the Tb silicide nanostructure growth when reusing substrates.

The upper image in Fig. 10(a) shows the result of a second nanowire preparation using the typical parameters for a closed Tb disilicide monolayer on planar substrates, but with a flash annealing cycle in between the two nanowire preparations. The nanowires are significantly wider than in the first preparation (shown in the lower image), now characterized by average widths of about 4.9 nm. Furthermore, the surface coverage with nanowires is much higher now. Thus, repeated preparations on the same substrates strongly influence the nanostructure growth.

On the one hand, this may pose problems regarding the comparability of different studies. For similar preparation parameters, wider nanowires were found on Si(557) substrates for Dy and Er than in the present paper for Tb [31,32], which may simply be traced back to the reuse of substrates. On the other hand, the history of the sample also represents an additional preparation parameter that may be useful to achieve the desired nanostructure growth. It is found, e.g., that nanowires on Si(335) grow more homogeneously when

a substrate is reused. Utilizing this approach, a homogeneous growth of well-defined nanowires with average widths of only 2.3 nm was achieved for submonolayer Tb coverages on Si(335) substrates [see Fig. 10(b)].

IV. CONCLUSION

In this paper, the growth of Tb-induced nanostructures on Si(*hhk*) substrates was analyzed with STM and the resulting structures were additionally identified using STS and XPS. Independently of the offcut direction, both the metallic Tb disilicide monolayer and the Tb-induced $2\sqrt{3}\times 2\sqrt{3}$ reconstructed submonolayer are formed. However, the Tb disilicide monolayer forms well-defined nanowires with straight edges only on Si(*hhk*) substrates with $h<k$. Very narrow metallic nanolines are also exclusively observed for this offcut direction. In general, narrower Tb disilicide nanostructures are observed for Si(*hhk*) substrates with increasing absolute values of the offcut angle with respect to Si(111). In this way, nanowires with an average width as low as 2.3 nm were grown. For such a strong confinement of a two-dimensional film in one direction, one may also expect a strong influence on the electronic structure, possibly leading to the observation of quasi-one-dimensional physics, which should be addressed in the future.

ACKNOWLEDGMENTS

We thank K. Horn and C. Papp for providing the UHV chamber for the photoemission measurements and BESSY II (Helmholtz-Zentrum Berlin) for beamtimes at the beamlines UE56/2 PGM-1 and PGM-2. J. Döhring is acknowledge for technical support. This work was supported by the DFG through FOR 1700 project E2.

[1] T. Giamarchi, Theoretical framework for quasi-one dimensional systems, Chem. Rev. **104**, 5037 (2004).
[2] S.-I. Tomonaga, Remarks on Bloch's method of sound waves applied to many-fermion problems, Prog. Theoret. Phys. **5**, 544 (1950).
[3] J. M. Luttinger, An exactly soluble model of a many-fermion system, J. Math. Phys. **4**, 1154 (1963).
[4] D. C. Mattis and E. H. Lieb, Exact solution of a many-fermion system and its associated boson field, J. Math. Phys. **6**, 304 (1965).
[5] F. D. M. Haldane, "Luttinger liquid theory" of one-dimensional quantum fluids. I. Properties of the Luttinger model and their extension to the general 1D interacting spinless Fermi gas, J. Phys. C: Solid State Phys. **14**, 2585 (1981).
[6] M. Bockrath, D. H. Cobden, J. Lu, A. G. Rinzler, R. E. Smalley, L. Balents, and P. L. McEuen, Luttinger-liquid behavior in carbon nanotubes, Nature **397**, 598 (1999).
[7] O. M. Auslaender, H. Steinberg, A. Yacoby, Y. Tserkovnyak, B. I. Halperin, K. W. Baldwin, L. N. Pfeiffer, and K. W. West, Spin-charge separation and localization in one dimension, Science **308**, 88 (2005).
[8] L. Dudy, J. D. Denlinger, J. W. Allen, F. Wang, J. He, D. Hitchcock, A. Sekiyama, and S. Suga, Photoemission spectroscopy and the unusually robust one-dimensional physics of lithium purple bronze, J. Phys.: Condens. Matter **25**, 014007 (2013).
[9] R. E. Peierls, *Quantum Theory of Solids* (Oxford University Press, London, 1955).
[10] S. Kagoshima, Peierls phase transition, Jpn. J. Appl. Phys. **20**, 1617 (1981).
[11] X. Zhu, J. Guo, J. Zhang, and E. W. Plummer, Misconceptions associated with the origin of charge density waves, Adv. Phys.: X **2**, 622 (2017).
[12] P. C. Snijders and H. H. Weitering, *Colloquium*: Electronic instabilities in self-assembled atom wires, Rev. Mod. Phys. **82**, 307 (2010).
[13] C. Preinesberger, S. Vandré, T. Kalka, and M. Dähne-Prietsch, Formation of dysprosium silicide wires on Si(001), J. Phys. D: Appl. Phys. **31**, L43 (1998).
[14] S. Appelfeller, M. Franz, H.-F. Jirschik, J. Große, and M. Dähne, The electronic structure of Tb silicide nanowires on Si(001), New J. Phys. **18**, 113005 (2016).
[15] S. Appelfeller, J. Heggemann, T. Niermann, M. Lehmann, and M. Dähne, Refined structure model of rare earth silicide nanowires on Si(001), Appl. Phys. Lett. **114**, 093104 (2019).
[16] C. Battaglia, H. Cercellier, C. Monney, M. G. Garnier, and P. Aebi, Stabilization of silicon honeycomb chains by trivalent adsorbates, Europhys. Lett. **77**, 36003 (2007).
[17] M. Franz, J. Große, R. Kohlhaas, and M. Dähne, Terbium induced nanostructures on Si(111), Surf. Sci. **637-638**, 149 (2015).
[18] H. W. Yeom, S. Takeda, E. Rotenberg, I. Matsuda, K. Horikoshi, J. Schaefer, C. M. Lee, S. D. Kevan, T. Ohta, T. Nagao, and S. Hasegawa, Instability and Charge Density Wave of Metallic Quantum Chains on a Silicon Surface, Phys. Rev. Lett. **82**, 4898 (1999).
[19] T. Frigge, B. Hafke, T. Witte, B. Krenzer, C. Streubühr, A. S. Syed, V. M. Trontl, I. Avigo, P. Zhou, M. Ligges, D. von der Linde, U. Bovensiepen, M. H. von Hoegen, S. Wippermann, A. Lücke, S. Sanna, U. Gerstmann, and W. G. Schmidt, Optically excited structural transition in atomic wires on surfaces at the quantum limit, Nature **544**, 207 (2017).
[20] C. W. Nicholson, A. Lücke, W. G. Schmidt, M. Puppin, L. Rettig, R. Ernstorfer, and M. Wolf, Beyond the molecular movie: Dynamics of bands and bonds during a photoinduced phase transition, Science **362**, 821 (2018).
[21] C. Blumenstein, J. Schäfer, S. Mietke, S. Meyer, A. Dollinger, M. Lochner, X. Y. Cui, L. Patthey, R. Matzdorf, and R. Claessen, Atomically controlled quantum chains hosting a Tomonaga-Luttinger liquid, Nat. Phys. **7**, 776 (2011).
[22] N. de Jong, R. Heimbuch, S. Eliëns, S. Smit, E. Frantzeskakis, J.-S. Caux, H. J. W. Zandvliet, and M. S. Golden, Gold-induced nanowires on the Ge(100) surface yield a 2D and not a 1D electronic structure, Phys. Rev. B **93**, 235444 (2016).
[23] T. Lichtenstein, Z. Mamiyev, E. Jeckelmann, C. Tegenkamp, and H. Pfnür, Anisotropic 2D metallicity: Plasmons in Ge(100)-Au, J. Phys.: Condens. Matter **31**, 175001 (2019).

[24] C. Tegenkamp, Vicinal surfaces for functional nanostructures, J. Phys.: Condens. Matter **21**, 013002 (2009).
[25] C. Tegenkamp, T. Ohta, J. L. McChesney, H. Dil, E. Rotenberg, H. Pfnür, and K. Horn, Coupled Pb Chains on Si(557): Origin of One-Dimensional Conductance, Phys. Rev. Lett. **100**, 076802 (2008).
[26] C. Brand, H. Pfnür, G. Landolt, S. Muff, J. H. Dil, T. Das, and C. Tegenkamp, Observation of correlated spin–orbit order in a strongly anisotropic quantum wire system, Nat. Commun. **6**, 8118 (2015).
[27] J. N. Crain, A. Kirakosian, K. N. Altmann, C. Bromberger, S. C. Erwin, J. L. McChesney, J.-L. Lin, and F. J. Himpsel, Fractional Band Filling in an Atomic Chain Structure, Phys. Rev. Lett. **90**, 176805 (2003).
[28] J. Aulbach, S. C. Erwin, R. Claessen, and J. Schäfer, Spin chains and electron transfer at stepped silicon surfaces, Nano Lett. **16**, 2698 (2016).
[29] C. Braun, C. Hogan, S. Chandola, N. Esser, S. Sanna, and W. G. Schmidt, Si(775)-Au atomic chains: Geometry, optical properties, and spin order, Phys. Rev. Mater. **1**, 055002 (2017).
[30] M. Dähne and M. Wanke, Metallic rare-earth silicide nanowires on silicon surfaces, J. Phys.: Condens. Matter **25**, 014012 (2013).
[31] M. Wanke, K. Löser, G. Pruskil, and M. Dähne, Structural and electronic properties of rare earth silicide nanowires on Si(557), Phys. Rev. B **79**, 155428 (2009).
[32] M. Wanke, M. Franz, M. Vetterlein, G. Pruskil, C. Prohl, B. Höpfner, P. Stojanov, E. Huwald, J. D. Riley, and M. Dähne, Electronic properties of dysprosium silicide nanowires on Si(557), J. Appl. Phys. **108**, 064304 (2010).
[33] T. Wagner, J. Aulbach, J. Schäfer, and R. Claessen, Au-induced atomic wires on stepped Ge(hhk) surfaces, Phys. Rev. Mater. **2**, 123402 (2018).
[34] S. Vandré, T. Kalka, C. Preinesberger, and M. Dähne-Prietsch, Flatband Conditions Observed for Lanthanide-Silicide Monolayers on *n*-Type Si(111), Phys. Rev. Lett. **82**, 1927 (1999).
[35] S. Vandré, T. Kalka, C. Preinesberger, and M. Dähne-Prietsch, Epitaxial growth and electronic structure of lanthanide silicides on *n*-type Si(111), J. Vac. Sci. Technol. B **17**, 1682 (1999).
[36] S. Vandré, C. Preinesberger, W. Busse, and M. Dähne, Conservation of flatband conditions for $DySi_2$ monolayers on *n*-type Si(111), Appl. Phys. Lett. **78**, 2012 (2001).
[37] M. Franz, S. Appelfeller, C. Prohl, J. Große, H.-F. Jirschik, V. Füllert, C. Hassenstein, Z. Diemer, and M. Dähne, Growth and electronic properties of Tb silicide layers on Si(111), J. Vac. Sci. Technol. A **34**, 061503 (2016).
[38] S. Sanna, C. Dues, W. G. Schmidt, F. Timmer, J. Wollschläger, M. Franz, S. Appelfeller, and M. Dähne, Rare-earth silicide thin films on the Si(111) surface, Phys. Rev. B **93**, 195407 (2016).
[39] A. M. Tokmachev, D. V. Averyanov, O. E. Parfenov, A. N. Taldenkov, I. A. Karateev, I. S. Sokolov, O. A. Kondratev, and V. G. Storchak, Emerging two-dimensional ferromagnetism in silicene materials, Nat. Commun. **9**, 1672 (2018).
[40] I. Goldfarb, F. Cesura, and M. Dascalu, Magnetic binary silicide nanostructures, Adv. Mater. **30**, 1800004 (2018).
[41] I. Horcas, R. Fernández, J. M. Gómez-Rodríguez, J. Colchero, J. Gómez-Herrero, and A. M. Baro, WSXM: A software for scanning probe microscopy and a tool for nanotechnology, Rev. Sci. Instrum. **78**, 013705 (2007).
[42] A. A. Baski, S. C. Erwin, and L. J. Whitman, The structure of silicon surfaces from (001) to (111), Surf. Sci. **392**, 69 (1997).
[43] A. Kirakosian, R. Bennewitz, J. N. Crain, T. Fauster, J.-L. Lin, D. Y. Petrovykh, and F. J. Himpsel, Atomically accurate Si grating with 5.73 nm period, Appl. Phys. Lett. **79**, 1608 (2001).
[44] S. Teys, K. Romanyuk, R. Zhachuk, and B. Olshanetsky, Orientation and structure of triple step staircase on vicinal Si(111) surfaces, Surf. Sci. **600**, 4878 (2006).
[45] A. N. Chaika, D. A. Fokin, S. I. Bozhko, A. M. Ionov, F. Debontridder, T. Cren, and D. Roditchev, Atomic structure of a regular Si(2 2 3) triple step staircase, Surf. Sci. **603**, 752 (2009).
[46] L. J. Pedri, L. Toppozini, and M. C. Gallagher, Au-induced nanofaceting and stoichiometry of the Si(775)-Au surface, Surf. Sci. **601**, 924 (2007).
[47] M. Kopciuszyński, P. Dyniec, R. Zdyb, and M. Jałochowski, Regular step distribution of the bare Si(553) surface, Phys. Rev. B **91**, 235420 (2015).
[48] I. Engelhardt, C. Preinesberger, S. K. Becker, H. Eisele, and M. Dähne, Atomic structure of thin dysprosium-silicide layers on Si(111), Surf. Sci. **600**, 755 (2006).
[49] M. Prietsch, A. Samsavar, and R. Ludeke, Structural and electronic properties of the Bi/GaP(110) interface, Phys. Rev. B **43**, 11850 (1991).
[50] R. I. G. Uhrberg, T. Kaurila, and Y.-C. Chao, Low-temperature photoemission study of the surface electronic structure of Si(111)7×7, Phys. Rev. B **58**, R1730 (1998).
[51] S. Chandola, E. Speiser, N. Esser, S. Appelfeller, M. Franz, and M. Dähne, Optical anisotropy of quasi-1D rare-earth silicide nanostructures on Si(001), Appl. Surf. Sci. **399**, 648 (2017).
[52] J. L. McChesney, A. Kirakosian, R. Bennewitz, J. N. Crain, J.-L. Lin, and F. J. Himpsel, Gd disilicide nanowires attached to Si(111) steps, Nanotechnol. **13**, 545 (2002).
[53] A. Kirakosian, J. L. McChesney, R. Bennewitz, J. N. Crain, J.-L. Lin, and F. J. Himpsel, One-dimensional Gd-induced chain structures on Si(1 1 1) surfaces, Surf. Sci. **498**, L109 (2002).
[54] S. M. Hus and H. H. Weitering, Formation of uni-directional ultrathin metallic YSi_2 nanowires on Si(110), Appl. Phys. Lett. **103**, 073101 (2013).